

# Circle Quasi-Cartograms: Dorling Cartograms with Edge Connections and Relaxed Overlap Conditions

Anonymous author(s)

Anonymous affiliation(s)

---

## 1 Abstract

Suppose we are given a graph,  $G = (V, E)$ , such that vertices have positive weights as well as geometric metadata, such as anchoring  $(x, y)$ -coordinates or geometric “home” regions. A *Dorling cartogram* is a way to visualize  $G$  where vertices are drawn as non-overlapping circles such that the circle for each vertex,  $v \in V$ , is drawn with size proportional to  $v$ 's weight and placed close to the anchoring location for  $v$ . Typically, the edges of  $G$  are not drawn in such visualizations, however; hence, adjacency information can be lost. In this paper, we introduce *circle quasi-cartograms*, which are modifications of Dorling cartograms where we join each pair of adjacent vertices with a line segment and we provide tunable parameters regarding the drawing, including the degree to which circles overlap. Specifically, we experimentally investigate force-directed circle quasi-cartogram drawing techniques for visualizing graphs where vertices have positive weights and geometric metadata under the the following constraints:

1. Each vertex,  $v \in V$  is drawn as a circle anchored to stay within or near a given geometric anchor region associated with  $v$ , as determined by an anchor force factor,  $\alpha$ .
2. We draw each edge as a line segment joining the centers of its circle endvertices.
3. Circle overlaps are determined by a tunable parameter,  $\rho$ .

Our goal is to preserve the geometric and topological information of the graph while still accurately representing the statistical data represented in vertex weights. Applications include population visualization, where we aim to accurately represent the size of populations in a given geographic region while also visualizing connections between regions. Our experiments indicate that these techniques allow us to trade off visualizing spatial and topological information at the cost of visualizing statistical information, which can be controlled by adjusting anchor and overlap forces.

**2012 ACM Subject Classification** Human-centered computing → Graph drawings; Theory of computation → Computational geometry

**Keywords and phrases** circle cartograms, force-directed graph drawing, geo-referenced data, geometric anchors

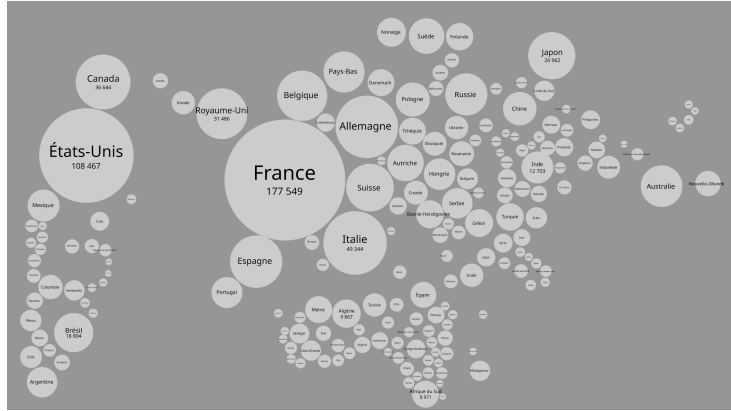
**Category** Short (Applied)

---

## 23 1 Introduction

Geometric vertex-weighted graphs, where vertices have associated geometric metadata, such as  $(x, y)$ -coordinates, geometric “home” regions, or multi-point associations, are common, but they pose challenging trade-offs when one wishes to visualize them. Cartograms have often been used to visualize such graphs, e.g., in the form of *value-by-area* maps, where vertices are drawn as geometric regions and adjacencies are represented by regions that touch; see, e.g., [1, 11, 13–16]. In a circle cartogram, which is also known as a “Dorling cartogram” [7], each vertex is represented as a circle proportional in size to its weight placed close to its geometric anchor so that circles do not overlap. See, e.g., Figure 1.

Typically, as shown in Figure 1, the edges of a graph visualized as a Dorling cartogram are not included. This is unfortunate, of course, since edge connections provide important information, such as topological relationships. Moreover, although the restriction to visualize vertices as non-overlapping circles is aesthetically pleasing, requiring that edges in a circle cartogram be represented only as touching circles severely limits the class of graphs that



32 **Figure 1** A Dorling cartogram of countries weighted by the number of links pointing to a country’s  
 33 article on the French Wikipedia. Image by Wikipedia user Moyogo, licensed under CC By-SA 3.0.

39 can be visualized. For example, if all the vertex weights are equal, then Dorling cartograms  
 40 where touching circles represent edges are equivalent to penny graphs, which cannot represent  
 41  $K_4$ , non-planar graphs, or a number of other interesting graphs; see, e.g., Eppstein [8].  
 42 Thus, in practice, if the circles in a circle cartogram do not overlap, and circles are drawn  
 43 with sizes proportional to their weights, then the visualization necessarily comes at the  
 44 cost of spatial and topological accuracy, as circles must be shifted without consideration of  
 45 the original topology. This is usually done via a force-directed algorithm that iteratively  
 46 repels overlapping circles while keeping them attracted to their initial position and/or edge  
 47 connections. As a result, Dorling cartograms often fail to preserve the viewer’s mental map  
 48 without additional labeling [16]. Work by Wei, Ding, Xu, Cheng, Zhang, and Wang [17]  
 49 aims to improve the topology of Dorling cartograms, but it fails to scale to larger graph  
 50 instances. Our work aims to relax the requirement to completely avoid circle overlaps, while  
 51 also explicitly drawing a graph’s edges as line segments joining the centers of the circles for  
 52 adjacent vertices, in order to obtain better geographical and topological accuracy.

53 **Additional Related Work.** Additional related work has considered anchored graph drawing,  
 54 where the input graph is assumed to have positional information that must be respected in  
 55 some way [12, 18]. Other work has also combined anchor forces with force-directed algorithms  
 56 to produce nice layouts that respect the initial geography [6].

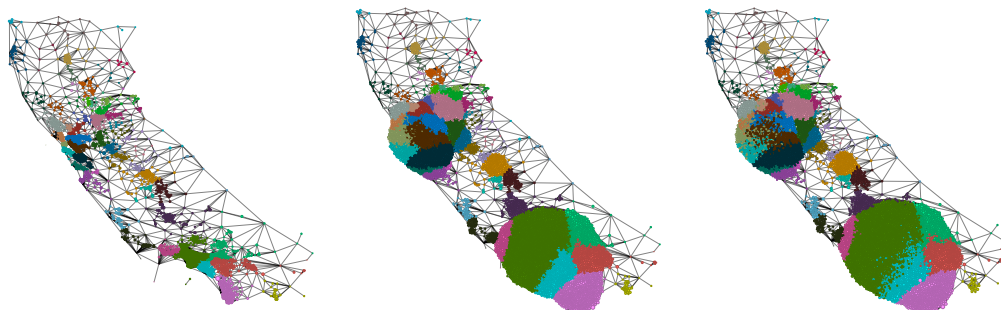
57 The standard force-directed algorithm in the literature is the Fruchterman-Reingold  
 58 algorithm, which treats edges as springs with attractive forces and makes the vertices repel  
 59 one another iteratively to produce a nice layout. However, this is slow on large graphs,  
 60 taking  $O(n^2)$  time per iteration where  $n$  is the number of vertices. Much work has been done  
 61 to produce faster force-directed algorithms, such as the Fast Multipole Multilevel Method  
 62 ( $FM^3$ ) by Hachul and Jünger [10]. The force-directed algorithm on which we build is the  
 63 Fast Multipole Embedder by Gronemann [9], which uses the same repulsive forces as in  
 64 Hachul and Jünger’s work, but modifies the attractive forces. These algorithms can handle  
 65 large graphs by approximating the repulsive force calculations between all pairs of nodes  
 66 using well-separated pair decompositions (WSPD) and multipole expansion [2–4].

67 **Our Results.** In this paper, we introduce *circle quasi-cartograms*, and we provide a  
 68 flexible force-directed algorithm for drawing circle quasi-cartograms with edge connections

69 explicitly represented and with relaxed overlap conditions, which are controlled by three  
 70 parameters: a node-scaling factor,  $\omega$ , an anchor force factor,  $\alpha$ , and an overlap force factor,  
 71  $\rho$ . Since achieving a graph drawing that preserves initial positions while avoiding any node  
 72 overlaps can be impossible, these three parameters are admittedly potentially in conflict with  
 73 one another. If, for instance, one sets the node-scaling factor  $\omega$  arbitrarily close to 0, then we  
 74 can trivially have no node overlap with the initial layout. If one sets the anchor force factor  
 75  $\alpha$  to 0, on the other hand, then we no longer have a geographical point of reference. And  
 76 finally, if one sets the overlap force factor  $\rho$  to 0, then we will inevitably have node overlaps  
 77 with any meaningful set of data. Hence, the desired parameters will be subject to tunable  
 78 trade-offs, which we explore in this paper.

79 For instance, by setting the overlap-force parameter  $\rho$  sufficiently high, our algorithm  
 80 produces circle quasi-cartograms that eliminate all circle overlaps. When the input is a  
 81 geographic map rather than an abstract graph, we first build its dual graph (connecting each  
 82 pair of adjacent regions) and then apply attractive forces along those dual edges, drawing  
 83 them explicitly in the quasi-cartogram to preserve regional topology. The anchor-force  
 84 parameter  $\alpha$  governs how strongly each circle is pulled toward its original geographic anchor:  
 85 reducing  $\alpha$  relaxes this pull, allowing nodes more freedom to reposition and overlap less.  
 86 Conversely, permitting controlled overlap by lowering  $\rho$  often yields layouts that better  
 87 preserve the map's adjacency structure, as illustrated in Figure 2.

88 In the example shown in Figure 2, the goal is to visualize county populations in California,  
 89 which is shown in their geographical locations in Figure 2a. We can represent a county in a  
 90 more granular fashion via its census tracts, which will allow its shape to morph according to  
 91 the constraints of its geography and topology once we run our algorithm. As census tracts  
 92 are designed to be relatively uniform in population, we can obtain a much more compact  
 93 visualization of the population this way. As it stands, we cannot visually see the population  
 94 size of these color-coded counties due to all the nodes overlapping each other. We show  
 95 two outputs of our algorithm: Figure 2b that has 1221 overlaps, and Figure 2c that has 9  
 96 overlaps. While the latter better represents the true size of these counties due to almost zero  
 97 node overlap, there is a fair amount of nodes spilling across county borders when this should  
 98 ideally only happen at the border. The former preserves this topology much better, however,  
 99 this comes at the cost of node overlaps that produce some minor cartographic error.



100 (a) Input geographic layout      (b)  $\omega = 100, \alpha = 1, \rho = 1$       (c)  $\omega = 100, \alpha = 1, \rho = 3$

101 ■ **Figure 2 CA.** (a) the dual graph of 8057 census tracts in California, where nodes are color-coded  
 102 by county and proportional to population. It has 83508 node overlaps. After running our algorithm,  
 103 (b) shows a drawing with 1221 node overlaps, and (c) shows a drawing with 9 node overlaps.

104 **2 The Force-Directed Algorithm**

105 **Fast Multipole Embedder.** The base force-directed algorithm we build upon is the Fast  
 106 Multipole Embedder of Gronemann [9]. As input, we are given a graph layout  $G = (V, E)$   
 107 where every vertex  $v \in V$  has a radius  $r_v$  and initial “anchor”  $xy$ -position vector  $\mathbf{q}_v$ . Let  
 108 two arbitrary vertices,  $u$  and  $v$ , be distance  $d_{uv} = |\mathbf{p}_u - \mathbf{p}_v|$  apart, where  $\mathbf{p}_u$  and  $\mathbf{p}_v$  are the  
 109 current  $xy$ -position vectors of  $u$  and  $v$  respectively. Then the magnitudes of the repulsive  
 110 force  $\mathbf{F}_{\text{rep}}(u, v)$  and the attractive force  $\mathbf{F}_{\text{attr}}(e)$  if edge  $e = (u, v) \in E$  exists will be:

$$111 \quad |\mathbf{F}_{\text{rep}}(u, v)| = \frac{c_r}{d_{uv}} \text{ and } |\mathbf{F}_{\text{attr}}(e)| = -c_a \cdot \log \frac{d_{uv}}{d_e} \cdot \frac{d_{uv}}{\deg(v)}. \quad (1)$$

112 Here  $c_r$  and  $c_a$  are constants, and  $d_e = r_u + r_v$  is the ideal edge length for edge  $e = (u, v)$ ,  
 113 when the two nodes  $u$  and  $v$  are tangent. Then each iteration of the algorithm will apply  
 114 these forces until we exceed the minimum number of iterations and the maximum force  
 115 falls below some threshold,  $\epsilon$ . However, calculating  $\mathbf{F}_{\text{attr}}(e)$  and  $\mathbf{F}_{\text{rep}}(u, v)$  exactly will take  
 116  $O(|E| + |V|^2)$  time per iteration, which becomes infeasible for large graphs.

117 To overcome this, the repulsive forces are approximated by grouping together far nodes  
 118 using a well-separated pair decomposition of all pairs of points [3]. This can be found in  
 119  $O(|V| \log |V|)$  time by constructing a hierarchical partition of the space into quadrants via  
 120 a quadtree data structure [4]. Then, the calculations themselves are approximated using  
 121 multipole expansion, which takes the first  $p$  terms (depending on the precision needed) of  
 122 the power series expansion of the forces. For  $t$  points, the approximate calculation will now  
 123 take  $O(pt)$  time, rather than the  $O(t^2)$  time needed for the exact calculation. The details of  
 124 these approximations (and the extent to which the error is bounded) can be found in [9].

125 **Anchor and Overlap Forces.** We apply two additional forces in each iteration, on top of  
 126 those supplied by the Fast Multipole Embedder algorithm. First, the anchor force acts like a  
 127 spring: it takes the displacement vector going from node  $u$ ’s current position  $\mathbf{p}_u$  to its initial  
 128 anchor position  $\mathbf{q}_u$ , multiplied by the *anchor factor*  $\alpha \in [0, 1]$  as seen in Figure 3a:

$$129 \quad \mathbf{F}_{\text{anchor}}(u) = \alpha(\mathbf{q}_u - \mathbf{p}_u) \quad (2)$$

130 We allow the anchor factor  $\alpha$  to range from  $[0, 1]$ , where  $\alpha = 0$  applies no anchor forces and  
 131  $\alpha = 1$  means that our anchor force pulls the node equal to its displacement from its original  
 132 location. There is no need for  $\alpha > 1$ , otherwise the force will “overshoot” the original anchor  
 133 position.

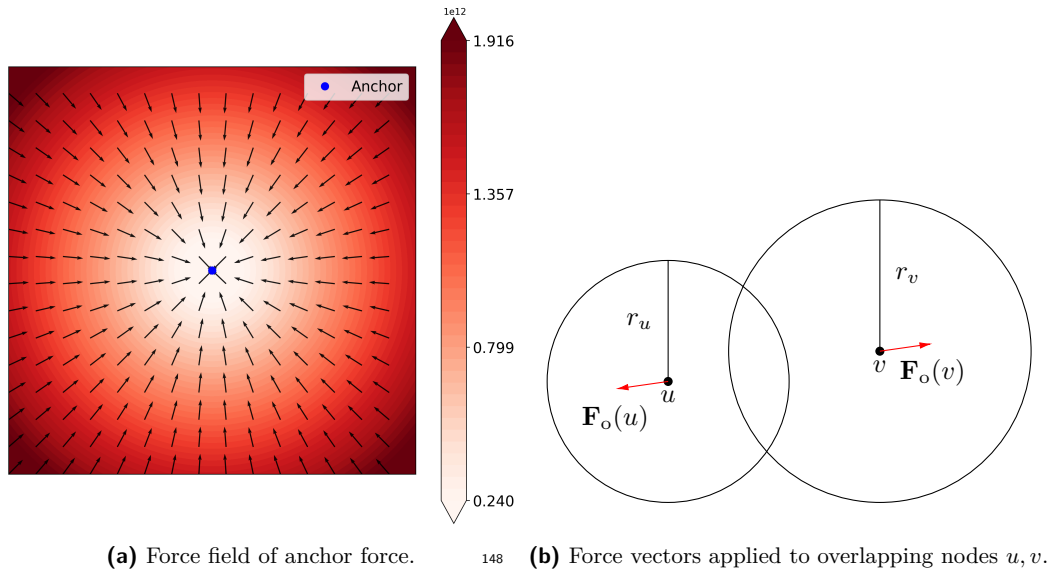
134 Second, we apply a force if two nodes  $u, v$  are overlapping, multiplied by an *overlap factor*  
 135  $\rho \geq 0$ , as seen in Figure 3b:

$$136 \quad \mathbf{F}_o(u) = \begin{cases} \rho \cdot \frac{r_u + r_v}{|\mathbf{p}_u - \mathbf{p}_v|} \cdot \frac{\mathbf{p}_u - \mathbf{p}_v}{|\mathbf{p}_u - \mathbf{p}_v|} & \text{if } d_{uv} < r_u + r_v \\ 0 & \text{else} \end{cases} \quad (3)$$

137 We note that while the overlap factor  $\rho$  can be unbounded, we will see that there is no need  
 138 to increase it once there are zero node overlaps.

139 Finally, each node  $u$  has some positive data weight  $w_u > 0$ , which will be used with the  
 140 *node-scaling factor*  $\omega$  to determine its radius  $r_u$ . Let  $w_{\max}$  be the maximum data weight.  
 141 Then we rescale the weights so that the radius of node  $u$  belongs in the range  $(0, \omega]$ :

$$142 \quad r_u = \omega \cdot \sqrt{\frac{w_u}{w_{\max}}} \quad (4)$$



149 ■ **Figure 3** Anchor and overlap forces applied in addition to the base force-directed algorithm.

143 If some input data weights are equal to 0, then we rescale the data to ensure that there  
 144 are only non-zero radii. Accordingly, the area of the circle corresponding to node  $u$  will be  
 145 proportional to its weight,  $w_u$ . Increasing the node-scaling factor  $\omega$  will spread the nodes as  
 146 they grow in size, but eventually this will out-scale the constraints of the initial layout.

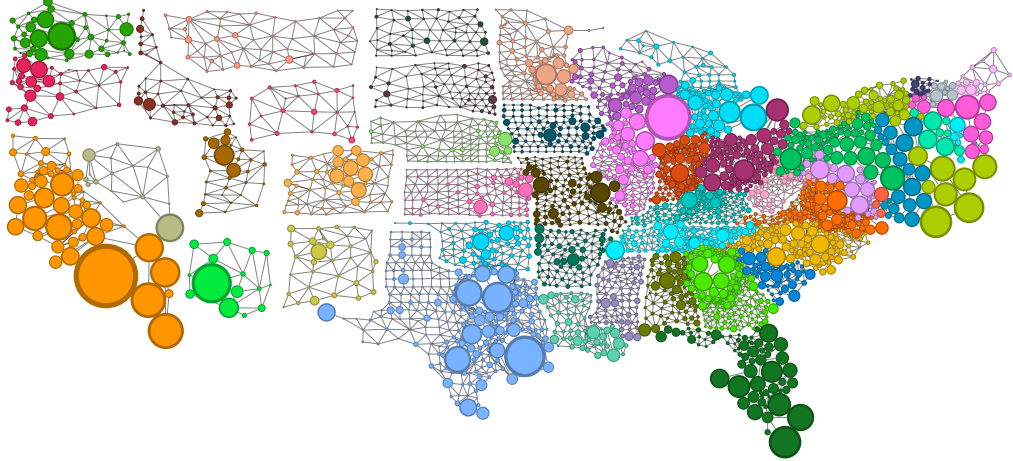
### 150 3 Experiments

151 We implemented our circle quasi-cartogram drawing algorithm using the Open Graph Drawing  
 152 Framework (OGDF) [5], and we ran experiments on a computer with 16GB RAM and a 12th  
 153 Gen Intel Core i5-12400F CPU. We experimentally studied the tradeoffs in various drawing  
 154 metrics as we adjust the three parameters of the algorithm. Specifically, we measure the  
 155 impact of various choices a node-scaling factor,  $\omega$ , an anchor force factor,  $\alpha$ , and an overlap  
 156 force factor,  $\rho$ , has on the following drawing metrics:

- 157 ■ The number of node overlaps
- 158 ■ The number of edge crossings
- 159 ■ The average edge length
- 160 ■ The average distance from initial anchor positions

161 We observe that the number of node overlaps can reach 0 by setting  $\rho$  high enough, which  
 162 often has high priority as it allows statistical data to be represented accurately in the  
 163 visualization. On the other hand, the number of edge crossings is not necessarily a priority  
 164 for visualizing geo-referenced data, but it is a natural graph layout metric to observe and can  
 165 be a proxy for the graph's topology. We mainly use geographic datasets for our experiments,  
 166 which naturally have few initial edge crossings. The average edge length can also be used as  
 167 a proxy metric for how well the geography was preserved compared to its value in the initial  
 168 layout (baseline). Finally, the average distance from the initial anchor positions is a key  
 169 metric that we do not want to increase too much from the baseline of 0 in the initial layout.

170 **Datasets.** Our first dataset, **USA**, is a graph of the 3108 counties of the 48 states in  
 171 the continental U.S. (which excludes Hawaii and Alaska). We added 7595 edges between



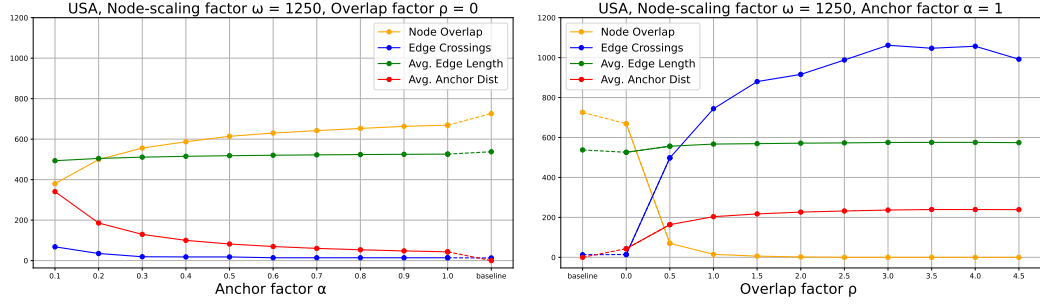
178 ■ **Figure 4** 2010 county populations of the continental USA, color-coded by states. It has 0 node  
179 overlaps with parameters  $\omega = 2500, \alpha = 1, \rho = 3$ .

172 adjacent counties if they belong to the same state, so the underlying graph has 48 connected  
173 components, one for each state (each with its own color in Figure 4). For a given county,  
174  $u$ , the initial position  $\mathbf{q}_u$  was set to the county’s centroid and its weight  $w_u$  was set to its  
175 population in the first dataset. The graph was constructed in this manner to preserve the  
176 topology within a state. The Northeast is the noteworthy region here, as it is the most  
177 densely populated region of the U.S. and thus we see the most mixing between states there.

180 Our second dataset, **CA**, is a dual graph of the 8057 census tracts in California, which  
181 form 22069 edges between adjacent tracts. For a given census tract,  $u$ , the initial position  
182  $\mathbf{q}_u$  is its centroid, and its weight  $w_u$  is its 2010 population. The baseline geographic layout  
183 is shown in Figure 2, along with two runs of the algorithm with  $\omega = 100, \alpha = 1, \rho = 1$  and  
184  $\omega = 100, \alpha = 1, \rho = 3$ . The census tract nodes are color coded by county, of which there are  
185 58 in California. We also note that Figure 2 can be viewed as a more granular representation  
186 of the county populations in California seen in Figure 4, which is the connected component  
187 in orange on the left.

188 **Parameter Evaluation.** We first consider fixing the node-scaling factor,  $\omega = 2500$ , while  
189 changing  $\alpha$  or  $\rho$ . We compare our algorithm against the “baseline” graph, which is simply  
190 the input graph layout for the **USA** dataset with node-scaling factor  $\omega = 2500$  that does  
191 not run our algorithm. Our results are shown in Figure 5, connected by a dashed line to  
192 the layouts for the baseline graph. We note that our algorithm’s output with parameters  
193  $\alpha = 1$  and  $\rho = 0$  is remarkably close to the baseline with respect to the four drawing metrics.  
194 Decreasing the anchor factor  $\alpha$  increases the average anchor distance as expected, with the  
195 slight benefit of fewer node overlaps. This makes sense as a layout that is less constrained  
196 to its initial layout provides more space for nodes. However, increasing the overlap factor  
197  $\rho$  from 0 achieves the same result of much fewer node overlaps but incurs higher average  
198 anchor distance and crossings almost immediately. In fact, we reach exactly 0 node overlaps  
199 at  $\rho = 3$ , and see that there is no real benefit to increasing  $\rho$  any further.

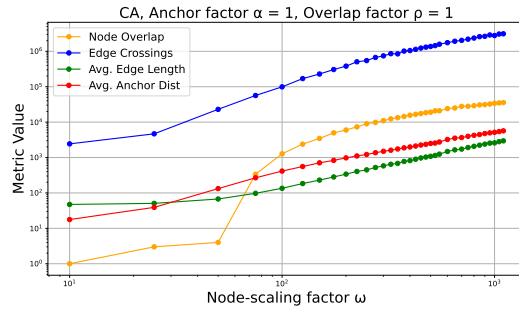
201 In the **CA** dataset, we observe the same trends when it comes to the trade-offs between  $\alpha$   
202 and  $\rho$  for a fixed node-scaling factor  $\omega$ . However, increasing  $\rho$  also leads to a steady increase



200 ■ **Figure 5** Plots showing graph metrics of USA county graph, fixing  $\omega$  and varying  $\alpha$  or  $\rho$ .

203 in the average edge length and anchor distance. We suspect that this was not as apparent in  
 204 the **USA** dataset (where both metrics seem to level off) due to the sparser connectivity of  
 205 the graph. Many of the connected components (the states of the U.S.) could not continue  
 206 expanding if surrounded by other states, whereas a single connected component would be  
 207 able to. Regardless, the number of edge crossings increased at a much faster rate and remains  
 208 the main trade-off for zero node overlaps when increasing  $\rho$ .

209 In the (log-log) plot shown in Figure 6, we see the effects of increasing the node-scaling  
 210 factor,  $\omega$ . All four graph metrics increase, so it is up to the user to decide at what point  
 211 the layout will still be meaningful. When  $\omega$  is large enough, it eventually out-scales the  
 212 original layout. Figure 2 shows the data point with  $\omega = 100, \alpha = 1, \rho = 1$ , which offers a  
 213 good compromise in preserving the geography while still visualizing the scale of the data.  
 214 For comparison, the layout that comes before the jump in node overlaps at  $\omega = 50$  is shown  
 215 by Figure 7 in the Appendix.



216 ■ **Figure 6** Log-log plot for the effect of the factor  $\omega$  on various graph qualities of the **CA** graph.

## 217 4 Conclusion

218 In this paper, we introduced a force-directed algorithm for drawing circle quasi-cartograms  
 219 that explicitly balances geographic fidelity, topological adjacency, and statistical accuracy  
 220 via controllable node overlap. We can achieve zero node overlaps mainly at the cost of  
 221 many edge crossings, with slight increases in the average edge length and anchor distance.  
 222 Although these edge crossings are often hidden by circles in congested parts of the layout, we  
 223 would like to reduce this metric in future work. If we permit some overlap, the topological  
 224 and geographical accuracy improves. An interesting future direction would be to model the  
 225 anchor locations more precisely than as anchor points.

---

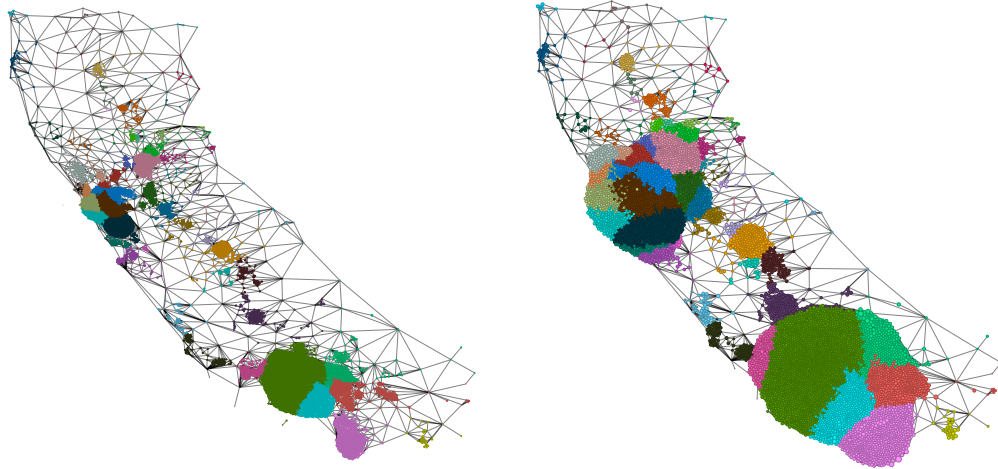
 226 ————— **References** —————

- 227    1 Md. Jawaherul Alam, Stephen G. Kobourov, and Sankar Veeramoni. Quantitative measures  
228    for cartogram generation techniques. *Computer Graphics Forum*, 34(3):351–360, 2015. doi:  
229    <https://doi.org/10.1111/cgf.12647>.
- 230    2 Josh Barnes and Piet Hut. A hierarchical  $O(N \log N)$  force-calculation algorithm. *Nature*,  
231    324(6096):446–449, December 1986. doi:[10.1038/324446a0](https://doi.org/10.1038/324446a0).
- 232    3 Paul B Callahan and S Rao Kosaraju. A decomposition of multidimensional point sets  
233    with applications to k-nearest-neighbors and n-body potential fields. *Journal of the ACM*,  
234    42(1):67–90, 1995.
- 235    4 Timothy M. Chan. Well-separated pair decomposition in linear time? *Information Processing  
236    Letters*, 107(5):138–141, 2008. doi:[10.1016/j.ipl.2008.02.008](https://doi.org/10.1016/j.ipl.2008.02.008).
- 237    5 Markus Chimani, Carsten Gutwenger, Michael Jünger, Gunnar W. Klau, Kerstin Klein, and  
238    Petra Mutzel. The open graph drawing framework (ogdf). In *Handbook of Graph Drawing  
239    and Visualization*, chapter 17. CRC Press, 2014.
- 240    6 Alvin Chiu, Ahmed Eldawy, and Michael T Goodrich. Polygonally anchored graph drawing.  
241    In *32nd International Symposium on Graph Drawing and Network Visualization (GD 2024)*,  
242    pages 52–1. Schloss Dagstuhl–Leibniz-Zentrum für Informatik, 2024. doi:[10.4230/LIPIcs.GD.2024.52](https://doi.org/10.4230/LIPIcs.GD.2024.52).
- 244    7 Daniel Dorling. Area cartograms: their use and creation. *The map reader: Theories of  
245    mapping practice and cartographic representation*, pages 252–260, 2011.
- 246    8 David Eppstein. Edge bounds and degeneracy of triangle-free penny graphs and squaregraphs.  
247    *Journal of Graph Algorithms and Applications*, 22(3):483–499, Sep. 2018. doi:[10.7155/jgaa.00463](https://doi.org/10.7155/jgaa.00463).
- 249    9 Martin Gronemann. Engineering the fast-multipole-multilevel method for multicore and simd  
250    architectures. *Master’s thesis. Technische Univ. Dortmund*, 2009.
- 251    10 Stefan Hachul and Michael Jünger. Drawing large graphs with a potential-field-based multilevel  
252    algorithm. In *Graph Drawing*, pages 285–295. Springer Berlin Heidelberg, 2005.
- 253    11 Jan-Hinrich Kämper, Stephen G. Kobourov, and Martin Nöllenburg. Circular-arc cartograms.  
254    In *2013 IEEE Pacific Visualization Symposium (PacificVis)*, pages 1–8, 2013. doi:[10.1109/PacificVis.2013.6596121](https://doi.org/10.1109/PacificVis.2013.6596121).
- 256    12 Kelly Lyons, Henk Meijer, and David Rappaport. Algorithms for cluster busting in anchored  
257    graph drawing. *Journal of Graph Algorithms and Applications*, 2(1):1–24, 1998.
- 258    13 Soeren Nickel, Max Sondag, Wouter Meulemans, Markus Chimani, Stephen Kobourov, Jaakko  
259    Peltonen, and Martin Nöllenburg. Computing stable Demers cartograms. In *Graph Drawing  
260    and Network Visualization*, pages 46–60, Cham, 2019. Springer International Publishing.
- 261    14 Sabrina Nusrat, Md. Jawaherul Alam, and Stephen Kobourov. Evaluating cartogram  
262    effectiveness. *IEEE Transactions on Visualization and Computer Graphics*, 24(2):1077–1090,  
263    2018. doi:[10.1109/TVCG.2016.2642109](https://doi.org/10.1109/TVCG.2016.2642109).
- 264    15 Sabrina Nusrat, Muhammad Jawaherul Alam, Carlos Scheidegger, and Stephen Kobourov. Cartogram  
265    visualization for bivariate geo-statistical data. *IEEE Transactions on Visualization  
266    and Computer Graphics*, 24(10):2675–2688, 2018. doi:[10.1109/TVCG.2017.2765330](https://doi.org/10.1109/TVCG.2017.2765330).
- 267    16 Sabrina Nusrat and Stephen Kobourov. The state of the art in cartograms. *Computer Graphics  
268    Forum*, 35(3):619–642, 2016. doi:[10.1111/cgf.12932](https://doi.org/10.1111/cgf.12932).
- 269    17 Zhiwei Wei, Su Ding, Wenjia Xu, Lu Cheng, Song Zhang, and Yang Wang. Elastic beam  
270    algorithm for generating circular cartograms. *Cartography and Geographic Information Science*,  
271    50(4):371–384, 2023. doi:[10.1080/15230406.2023.2196732](https://doi.org/10.1080/15230406.2023.2196732).
- 272    18 Hsiang-Yun Wu, Martin Nöllenburg, and Ivan Viola. Multi-level area balancing of clustered  
273    graphs. *IEEE Transactions on Visualization and Computer Graphics*, 28(7):2682–2696, 2022.  
274    doi:[10.1109/TVCG.2020.3038154](https://doi.org/10.1109/TVCG.2020.3038154).

275

## 5 Appendix

280 The first two datasets **USA** and **CA** can be found at [https://people.csail.mit.edu/ddeford/dual\\_graphs.html](https://people.csail.mit.edu/ddeford/dual_graphs.html). Below we show the difference when increasing the node-scaling  
 281 factor  $\omega$ , which is a trade-off between geographical accuracy and the scale of data. Orange  
 282 County (color teal, unfortunately) and San Diego County (color pink) in Southern California  
 283 do not seem to border in Figure 7a but do in Figure 7b, fully connecting the 5 major counties  
 284 of Southern California into one big population “blob”.



276

(a)  $\omega = 50, \alpha = 1, \rho = 1$ 

277

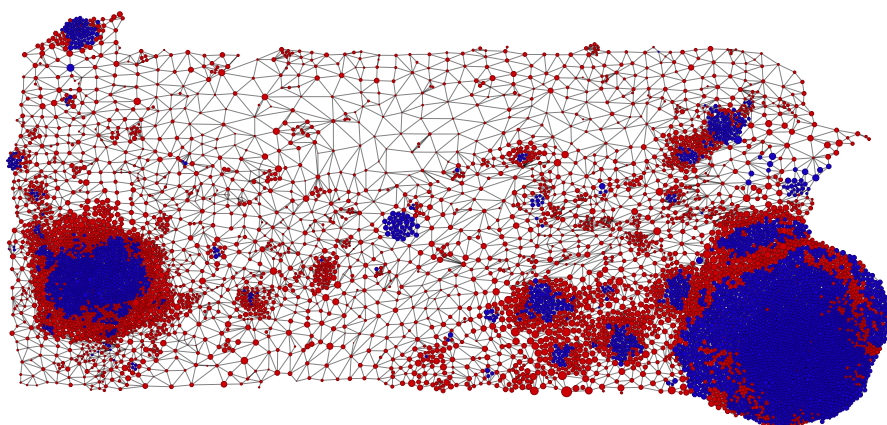
(b)  $\omega = 100, \alpha = 1, \rho = 1$ 

278

**Figure 7** The effect of varying the node-scaling factor  $\omega$  is shown on the **CA** dataset. (a) has 4  
 279 node overlaps, while (b) has 1221 node overlaps.

285

We also show a third dataset **PA** in Figure 8, which can be found at <https://github.com/mggg/GerryChain/blob/main/docs/user/quickstart.rst>:



286

**Figure 8** 2016 U.S. Election results of Pennsylvania. Its 8921 voting tabulation districts  
 287 are represented as red nodes if Republican-majority or blue nodes if Democrat-majority, scaled  
 288 proportional to the number of winning votes. 40 node overlaps with parameters  $\omega = 50, \alpha = 1, \rho = 1$ .

290